Fully automated large-area OCT scanning procedure for a combined OCT-Raman system

Rene Riha,[1,*] Manuel Marques,[1] Adrian Bradu,[1] Radu Boitor,[2] Nehal Atallah,[2] Ioan Notingher[2] and Adrian Podoleanu[1]

[1] *Applied Optics Group, School of Engineering, Mathematics and Physics, University of Kent, Canterbury, CT2 7NH, UK*

[2] *School of Physics and Astronomy, University of Nottingham, Nottingham, NG7 2RD, UK*

[*] *rr406@kent.ac.uk*

Abstract: We present a fully automated large-area OCT imaging procedure with real-time refocusing integrated with a combined OCT-Raman system. Scanning along the *x*-axis is achieved using a single galvanometer paired with a telecentric lens. Scanning along the *y*-axis is accomplished by translating a sample with a motorised horizontal stage over a much larger lateral size. The same translation stage is also moved along the *y*-axis to repeat the scanning over connecting columns. Automated refocusing at equidistant intervals along the *y*-axis is performed using a motorised vertical stage, which carries the combined OCT-Raman imaging head. We also perform spatial calibration between the OCT and Raman optics to enable automated focusing of the Raman optics onto the sample surface. The procedure is validated on a large 5 cm × 5 cm biological sample, with assessment of scanning time and other imaging parameters. A surface map is generated to guide the subsequent Raman measurements, and a targeted Raman measurement is performed on selected sites on the sample. This combined OCT-Raman system is designed for fully automated intra-operative breast cancer diagnosis, integrating OCT imaging, AI-based classification, and Raman spectroscopy. © 2026 The Author(s)

1. Introduction

Optical coherence tomography (OCT) has become a highly relevant non-invasive imaging technique in biomedical optics, industry, or art conservation [1]. OCT reconstructs depth information by analysing interferometric signals from backscattered light.

While conventional OCT has been proven valuable in examining small regions up to 1 cm × 1 cm with exceptional detail, it may not always be ideal for capturing images of larger areas, such as whole tissue sections, large industrial samples, or large works of art. In dermatology, skin conditions often spread over large areas [2]. OCT of large breast tissues samples can assist surgeons in intra-operative diagnoses [3]. Large-area imaging of non-biological samples proves advantageous in detecting hidden defects over the entire sample surface [4]. Large-area imaging also facilitates quantifying optical parameters for conservation and restoration purposes of the art works [5]. To address large-area imaging, system with robotic arms [6], motorised stages [5], or full-field OCT (FF-OCT) systems with megapixel cameras [3] have been developed.

We present a fully automated large-area OCT scanning procedure that combines a single galvanometer paired with a telecentric lens and a motorised horizontal and vertical stage. This procedure is used to generate a surface map that guides subsequent Raman measurements in the combined OCT–Raman system.

2. Methods

The combined OCT-Raman imaging instrumentation is displayed in Fig. 1 on the left. A sample is placed on a motorised computer-controlled horizontal stage (Prior H117P1, 11 cm × 7 cm maximum travel range, 1 cm/s maximum speed), and the combined imaging head is attached to a motorised computer-controlled vertical stage (Zaber X-LDA020A-AE53ZJ2D12, 4 cm maximum travel range, 60 cm/s maximum speed). The OCT optics comprises a single galvanometer (Thorlabs QS7Y-AG, ±22.5° maximum scanning angle) and a large field of view telecentric lens (Thorlabs LSM54-1050, 54 mm focal length, 18 × 18 mm^2 field of view). The OCT and Raman optics (Leica Germany N PLAN L 50x/0,50) are mounted together in a cage system.

The principle of the large area OCT scanning procedure is depicted in Fig. 1 on the right. Along the *x*-axis, the beam is scanned over the sample surface across the field of view Δx_g using a combination of the galvanometer and the telecentric lens. The *x*-scanning follows a triangular pattern with a period given by $T_{\text{B-scan}} = 1/f_{\text{B-scan}}$,

where $f_{\text{B-scan}}$ is the B-scan frequency. Half of this period is dedicated to the B-scan acquisition, while the other half is reserved for the galvanometer fly-back and signal processing. Along the y-axis, the beam remains stationary and scanning along this axis is achieved by moving the horizontal stage. To keep the sample surface in the focus, the surface depth is measured and height of the scanning head is adjusted at every refocusing distance Δy_{f} along the y-axis using the motorised vertical stage. The parameters Δx_{g} and Δy_{f} can be adjusted based on the expected roughness of the sample surface.

In this way, a refocused raster column j with the size equal to $\Delta x_{\text{g}} \times I\Delta y_{\text{f}}$, where I is the number of refocusing points, is obtained. The x- and y-axes pixel sizes are given by $\delta x = 2\Delta x_{\text{g}} f_{\text{B-scan}}/f_{\text{s}}$ and $\delta y = 2v_{\text{hor-stage}}/f_{\text{B-scan}}$, respectively, where f_{s} is the sweep frequency of the employed light source, and $v_{\text{hor-stage}}$ is the speed of the horizontal stage. The transition from column j to column $j+1$ is accomplished by moving the horizontal stage in the x-direction by Δx_{g}, and repeating the scanning process along the y-axis with refocusing every Δy_{f}. The starting y-coordinate of the column $j+1$ is the ending y-coordinate of the column j, which saves scanning time compared to returning the stage to zero y-coordinate after each column is scanned. The entire raster scan consists of J columns, covering a total area of $\Delta x \times \Delta y = J\Delta x_{\text{g}} \times I\Delta y_{\text{f}}$.

To enable automated focusing of the Raman optics onto a selected point on the sample surface, a horizontal and vertical calibration between the OCT and Raman optics must be performed. The Raman surface coordinates x_{Raman}, y_{Raman}, and $z_{\text{Raman}}(x_{\text{Raman}}, y_{\text{Raman}})$ are then given by:

$$x_{\text{Raman}} = x_{\text{OCT}} + \Delta x_{\text{obj}}, \quad y_{\text{Raman}} = y_{\text{OCT}}, \quad z_{\text{Raman}}(x_{\text{Raman}}, y_{\text{Raman}}) = z_{\text{OCT}}(x_{\text{OCT}}, y_{\text{OCT}}) + z_{\text{ver-stage}} + \Delta z_{\text{obj}}, \quad (1)$$

where x_{OCT}, y_{OCT}, and $z_{\text{OCT}}(x_{\text{OCT}}, y_{\text{OCT}})$ are surface coordinates obtained in OCT, $\Delta z_{\text{ver-stage}}$ denotes the vertical stage position at which a B-scan was taken, and Δx_{obj} and Δz_{obj} are the objectives offsets along the x- and z-axes, respectively.

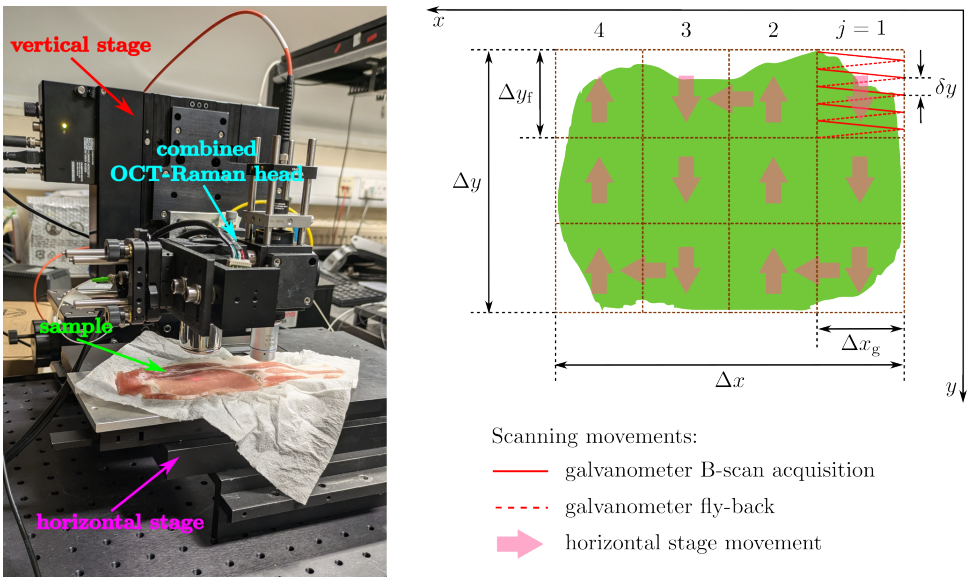

Fig. 1. **Left:** Photo of the combined OCT-Raman instrumentation. **Right:** Principle of the large-area OCT scanning procedure. Δx: x-axis scanning size, Δy: y-axis scanning size, Δx_{g}: galvanometer field of view, Δy_{f}: y-axis refocusing distance, δy: y-axis pixel resolution.

3. Results

For a preliminary testing, the large-area OCT scanning procedure was used to scan 5 cm × 5 cm area on a bacon (red square in Fig. 2(a)). The lateral pixel sizes were adjusted to 10 and 20 µm along the x- and y-axes, respectively. The whole raster consisting of total 28,000 B-scans took approximately 6 mins, including saving the B-scans. The B-scans were obtained using the Leader-Follower interferometry [7], with 20 ms acquisition time per B-scan. The stitched depth average C-scan and surface map $z_{\text{raman}}(x, y)$ for Raman measurements are displayed in Figs. 2(b) and 2(c), respectively. The examples of B-scan of a muscle tissue (blue line in Fig. 2(a)) and a fat tissue (green line in Fig. 2(a)) are displayed in Figs. 2(d) and 2(e), respectively. Finally, targeted Raman measurement of the fat tissue is displayed in Fig. 2(f).

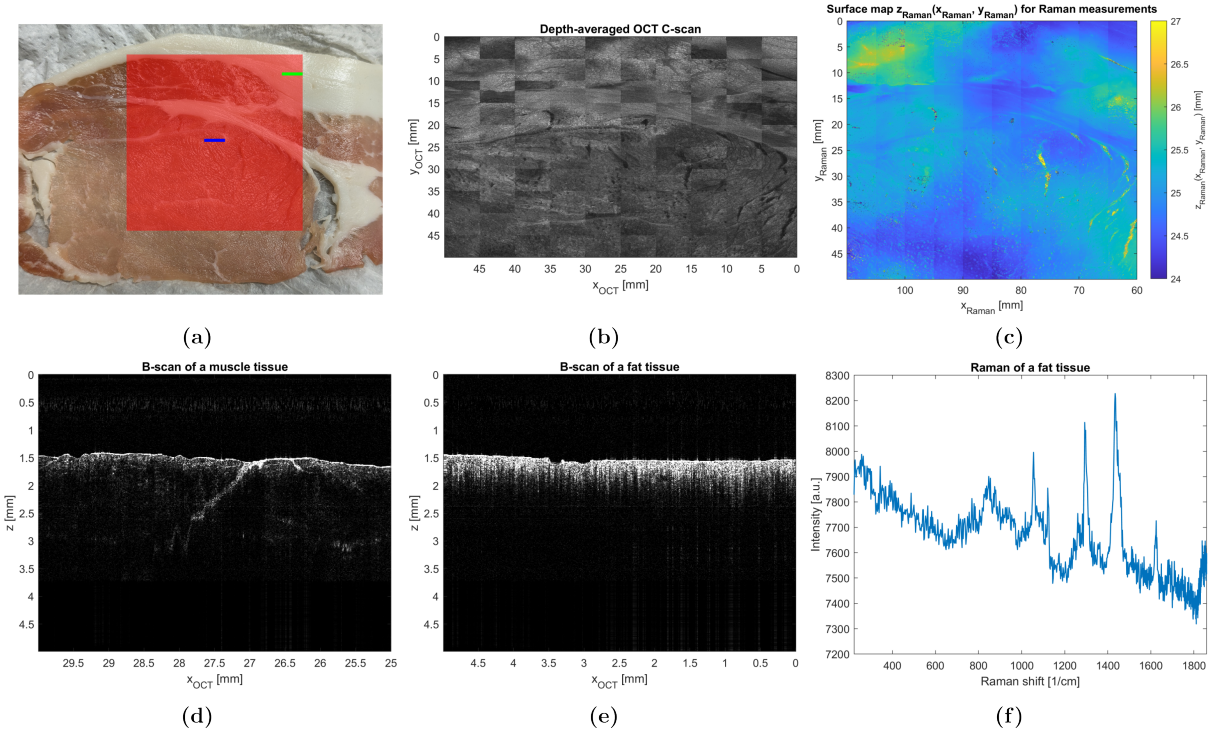

Fig. 2. **(a)** OCT scanned 5 cm × 5 cm area on a bacon. **(b)** Depth-averaged OCT C-scan of the area. **(c)** Calibrated surface map for Raman measurements. **(d)** B-scan of a muscle tissue (blue line in Fig. 2(a)). **(e)** B-scan of a fat tissue (green line in Fig. 2(a)). **(f)** Targeted Raman measurement on the fat tissue.

4. Conclusion

We present a fully automated large-area OCT imaging procedure with real-time refocusing that combines a single galvanometer and a motorised horizontal and vertical stage. With spatially calibrated OCT and Raman optics in the combined head, the procedure is validated on a large 5 cm × 5 cm biological sample, from which a surface map is generated to guide subsequent Raman measurements. This large-area scanning procedure was developed for fully automated intraoperative breast cancer diagnosis, integrating OCT imaging, AI-based classification, and Raman spectroscopy.

Acknowledgments

This work was supported by the Medical Research Council (MR/Y008731/1). AB acknowledges funding from the Royal Society (PARSOCT, RGS/R1/221324), the Academy of Medical Sciences, the Wellcome Trust, BEIS, the British Heart Foundation, and Diabetes UK (Springboard Award SBF007100162). MJM and AP acknowledge support from King's College, Moorfields Eye Hospital, and NIHR (202879). MJM, AB, and AP acknowledge BBSRC Impact Accelerator Account support. MJM also acknowledges Royal Society funding (RG/R2/232087).

References

1. W. Drexler and J. G. Fujimoto, eds., *Optical Coherence Tomography: Technology and Applications*, Springer, 2nd ed., 2015.
2. A. S. Aldahan, L. L. Chen, R. M. Fertig, J. Holmes, V. V. Shah, S. Mlacker, V. M. Hsu, K. Nouri, and A. Tosti, "Vascular features of nail psoriasis using dynamic optical coherence tomography," *Skin Appendage Disorders* **2**(3-4), pp. 102–108, 2017.
3. O. Assayag, M. Antoine, B. Sigal-Zafrani, M. Riben, F. Harms, A. Burcheri, B. Le Conte de Poly, and C. Boccara, "Large field, high resolution full-field optical coherence tomography: A pre-clinical study of human breast tissue and cancer assessment," *Technology in Cancer Research & Treatment* **13**(5), pp. 455–468, 2014.
4. B. He, Y. Zhang, L. Zhao, Z. Sun, X. Hu, Y. Kang, L. Wang, Z. Li, W. Huang, Z. Li, G. Xing, F. Hua, C. Wang, P. Xue, and N. Zhang, "Robotic-oct guided inspection and microsurgery of monolithic storage devices," *Nature Communications* **14**(1), p. 5701, 2023.

5. T. Callewaert, J. Guo, G. Harteveld, A. Vandivere, E. Eisemann, J. Dik, and J. Kalkman, "Multi-scale optical coherence tomography imaging and visualization of vermeer's girl with a pearl earring," *Opt. Express* **28**, pp. 26239–26256, Aug 2020.
6. S. Lotz, M. Göb, S. Böttger, L. Ha-Wissel, J. Hundt, F. Ernst, and R. Huber, "Large area robotically assisted optical coherence tomography (lara-oct)," *Biomed. Opt. Express* **15**, pp. 3993–4009, Jun 2024.
7. S. Rivet, M. Maria, A. Bradu, T. Feuchter, L. Leick, and A. Podoleanu, "Complex master slave interferometry," *Opt. Express* **24**, pp. 2885–2904, Feb 2016.